ROYAL SOCIETY OPEN SCIENCE

rsos.royalsocietypublishing.org

Research

Cite this article: Pan X, Xu Z, Zheng Y, Huang T, Li L, Chen Z, Rao W, Chen S, Hong X, Guan X. 2017 The adsorption features between insecticidal crystal protein and nano-$Mg(OH)_2$. *R. Soc. open sci.* **4**: 170883.
http://dx.doi.org/10.1098/rsos.170883

Received: 13 July 2017
Accepted: 31 October 2017

Subject Category:
Chemistry

Subject Areas:
behaviour/biotechnology/chemical biology

Keywords:
insecticidal protein, nano-$Mg(OH)_2$, adsorption isotherm, adsorption kinetics, adsorption thermodynamics

Authors for correspondence:
Xiong Guan
e-mail: guanxfafu@126.com

This article has been edited by the Royal Society of Chemistry, including the commissioning, peer review process and editorial aspects up to the point of acceptance.

THE ROYAL SOCIETY PUBLISHING

The adsorption features between insecticidal crystal protein and nano-$Mg(OH)_2$

Xiaohong Pan[1,2], Zhangyan Xu[1], Yilin Zheng[1], Tengzhou Huang[1], Lan Li[1], Zhi Chen[1], Wenhua Rao[1], Saili Chen[1], Xianxian Hong[1] and Xiong Guan[1,2]

[1]State Key Laboratory of Ecological Pest Control for Fujian and Taiwan Crops and Key Lab of Biopesticide and Chemical Biology, Ministry of Education, College of Plant Protection, College of Resources and Environmental Sciences, Fujian Agriculture and Forestry University, Fuzhou, Fujian 350002, People's Republic of China
[2]Fujian-Taiwan Joint Center for Ecological Control of Crop Pests, Fuzhou, Fujian 350002, People's Republic of China

XG, 0000-0003-3505-7464

Nano-$Mg(OH)_2$, with low biological toxicity, is an ideal nano-carrier for insecticidal protein to improve the bioactivity. In this work, the adsorption features of insecticidal protein by nano-$Mg(OH)_2$ have been studied. The adsorption capacity could reach as high as 136 mg g^{-1}, and the adsorption isotherm had been fitted with Langmuir and Freundlich models. Moreover, the adsorption kinetics followed a pseudo-first or -second order rate model, and the adsorption was spontaneous and an exothermic process. However, high temperatures are not suitable for adsorption, which implies that the temperature would be a critical factor during the adsorption process. In addition, FT-IR confirmed that the protein was adsorbed on the nano-$Mg(OH)_2$, zeta potential analysis suggested that insecticidal protein was loaded onto the nano-$Mg(OH)_2$ not by electrostatic adsorption but maybe by intermolecular forces, and circular dichroism spectroscopy of Cry11Aa protein before and after loading with nano-$Mg(OH)_2$ was changed. The study applied the adsorption information between Cry11Aa and nano-$Mg(OH)_2$, which would be useful in the practical application of nano-$Mg(OH)_2$ as a nano-carrier.

1. Introduction

Bacillus thuringiensis (Bt), a spore-forming Gram-positive strain, is widely used as a biopesticide, and can form insecticidal crystal protein (including Cry and Cyt proteins) during the stationary phase of growth [1–4]. But there are some disadvantages when the Bt product is applied in the field, such as the active

ingredients being rapidly inactivated by ultraviolet (UV) light or degraded by other microorganisms [5–7], which hinder its effective application. There are several ways to prevent its inactivation and degradation, such as encapsulation, adding a coating agent and ultraviolet stabilizers, or gene regulation [8–11]; however, the additives have poor compatibility or stability, which might increase risk to the environment of the biopesticide.

In recent years, numerous studies have focused on nanomaterials because nanoparticles possess strong adsorption capacity, high specific surface area and specific physicochemical properties [12–14]. Nanoparticles can be used as excellent nano-carriers in nanodrug delivery systems, which can improve the utilization rates and promote direct drug diffusion [12,15]. Additionally, nanoparticles are also widely used for biopesticides. It was reported that porous hollow silica nanoparticle (PHSN) carriers exhibited remarkable UV-shielding properties for avermectin, and the avermectin could be released slowly after loading on PHSN carriers [16]. Qin *et al*. [12] prepared nanoscale chitinases by immobilizing Bt chitinases onto the surface of silica nanoparticles through electrostatic adsorption and covalent binding; the nanoparticles could synergistically enhance the nematicidal effect, which implied that silica nanoparticles can serve as an efficient nano-carrier. Also, mesoporous silicon particles have been applied in the protection and delivery of the anthelmintic protein Cry5B [17]. Most of the previous reports aim to improve the properties of the biopesticide by effects such as UV shielding and control of release and biological activity. However, it is also essential to understand the adsorption features, because the adsorption behaviour will reflect the adsorption affinity and efficiency, and regulation of the adsorption process might enhance the insecticidal activity and facilitate the practical application of nanomaterials in biopesticide use.

Nano-$Mg(OH)_2$ is an environmentally friendly material; it is widely used as an adsorbent in wastewater removal [18–20] with low biological toxicity [21,22]. Our previous studies indicated that Cry11Aa protein had high activity against disease vector mosquitoes, and the Cry11Aa protein loaded onto nano-$Mg(OH)_2$ had even stronger toxicity toward mosquitoes [23]. But the adsorption features of Cry11Aa by nano-$Mg(OH)_2$ still need further study in order to develop a new mosquitocide. Herein, we applied adsorption experiments (such as adsorption isotherms, kinetic and thermodynamics analysis) to investigate the adsorption characteristics of nano-$Mg(OH)_2$ toward insecticidal protein. The understanding of the adsorption behaviour might be useful to regulate the adsorption in practical applications.

2. Material and methods

2.1. Cry11Aa and nano-$Mg(OH)_2$

The nano-$Mg(OH)_2$ was synthesized by coprecipitation of magnesium chloride hexahydrate ($MgCl_2{\cdot}6H_2O$) and sodium hydroxide (NaOH) as described in previous studies [24] with minor modification. Briefly, 0.70 g $MgCl_2{\cdot}6H_2O$ was added into 10 ml ddH_2O for dissolution, and 0.28 g NaOH was dissolved in 10 ml ddH_2O, then the dissolved NaOH was slowly added into $MgCl_2{\cdot}6H_2O$ solution with continuous stirring overnight. Finally, the mixture was centrifuged at 10 000*g* for 5 min and washed with ddH_2O three times for further characterization. The Cry11Aa was extracted from Bt LLP29 strain according to the method described by Helassa [25].

2.2. Adsorption isotherms

The adsorption isotherm experiments were performed at 4°C. The concentration of Cry11Aa ranged from 0.068 to 0.68 mg ml^{-1}, and the concentration of nano-$Mg(OH)_2$ was set at 10 g l^{-1}. Experiments were performed with ultrasonication for 30 min, which was found to be sufficient time for the mixture to reach adsorption equilibrium. After equilibrium, the supernatant was extracted by centrifugation. Then the concentration of Cry 11Aa protein was measured, and the adsorption capacity was calculated.

2.3. Adsorption kinetic analysis

Nano-$Mg(OH)_2$ 0.01 g was added to 1 ml protein solution (0.68 mg ml^{-1}) with ultrasonication at 4°C. For time series experiments, 50 µl aliquots were extracted at the appropriate time intervals, centrifuged at 6000*g* for 3 min and the supernatant was recovered. The remaining protein concentration was measured.

2.4. Adsorption thermodynamics

Nano-$Mg(OH)_2$ 0.01 g was added to 1 ml of 0.68 mg ml^{-1} protein solution and ultrasonicated for 2 h at a series of fixed temperatures (20°C, 25°C and 30°C) until adsorption equilibrium was reached. The protein concentration of the supernatant was measured and the adsorption capacity of was calculated.

2.5. The desorption experiment

The desorption experiment was conducted in a simulated natural environment (pH = 5.6). 1 ml of 30 mM MES ($C_6H_{13}NO_4S$) medium was added to the loaded sample (Cry11Aa-$Mg(OH)_2$) in a 2 ml centrifuge tube, and the sample was incubated at room temperature with gentle agitation. Then the supernatant was collected every 12 h by centrifugation followed by addition of fresh MES medium, for a total of seven times. The concentration of Cry11Aa protein in the supernatant was measured in order to calculate the desorption rate of Cry11Aa from nano-$Mg(OH)_2$.

2.6. FT-IR, zeta-potential and circular dichroism analyses

The nano-$Mg(OH)_2$ after Cry protein loading (0.01 g nano-$Mg(OH)_2$: 1 ml protein) was separated into supernatant and precipitate by centrifugation, and the precipitate was dried by freeze drying at −80°C. Then the nano-$Mg(OH)_2$ and nano-$Mg(OH)_2$ loaded with protein were prepared in a KBr pellet with a sample/KBr ratio of 1:100, and the thin pellets were analyzed using a PerkinElmer Spectrum One FT-IR spectrometer in the range of 4000–400 cm^{-1}.

The surface charge of the nanoparticles before and after protein loading was measured in 50 mM citrate buffer with a Malvern Instruments Zetasizer ZS90 instrument. For each sample, an appropriate amount of undiluted solution was placed into the cuvette, and an average zeta potential value was obtained from three individual measurements. The solution media was set as water for all zeta potential measurements.

The Brunauer-Emmett-Teller (BET) surface area of the nano-$Mg(OH)_2$ was measured using a Micrometrics ASAP 2020 system. The BET surface area, using the adsorption data, was determined by a multipoint BET method, and the relative pressure (P/P^0) ranged from 0.01 to 1.0.

The circular dichroism (CD) spectra of Cry11Aa protein before and after loading onto nano-$Mg(OH)_2$ were recorded on a CD spectropolarimeter (Chirascan^{TM}, Applied Photophysics Ltd, UK). The samples were measured in a 1 mm pathlength quartz cell at 37°C. The spectra were scanned between 195 and 260 nm, three scans were accumulated at a scanning speed of 60 nm min^{-1} and a time constant of 0.5 s, and the spectra were averaged over three consecutive scans.

3. Results

3.1. Effect of protein concentration and adsorption isotherm study

The adsorption capacity between Cry11Aa and nano-$Mg(OH)_2$ was evaluated by equilibrium experiments (figure 1), and the Langmuir and Freundlich models were applied to understand the adsorption mechanism. The calculations were described as follows:

$$\text{Langmuir}: \quad Q_e = \frac{Q^0 b C_e}{1 + bC_e} \tag{3.1}$$

$$\text{Freundlich}: \quad Q_e = kC_e^{\frac{1}{n}} \tag{3.2}$$

where Q_e represents the adsorbed capacity at equilibrium, Q_0 is maximum amount or the saturated adsorption amount (mg g^{-1}), C_e is the equilibrium concentration in the solution (mg l^{-1}), b is the Langmuir constant (l/mg) which relates to the binding strength, and n and k are the Freundlich constants which relate to the biosorption intensity and biosorption capacity, respectively.

As revealed in table 1, the Langmuir and Freundlich isotherm models are both appropriate to depict the adsorption process based on R^2 value, and the saturated adsorption capacity of Cry protein was 100.2 mg g^{-1} (Q^0). Meanwhile, the relative larger value of the b constant indicated a favourable adsorptive process of Cry protein on nano-$Mg(OH)_2$ according to the Langmuir fitting results, which was also confirmed by the Freundlich constant n (n lies between 1 and 10, indicating that the adsorbate is favourably adsorbed [26]).

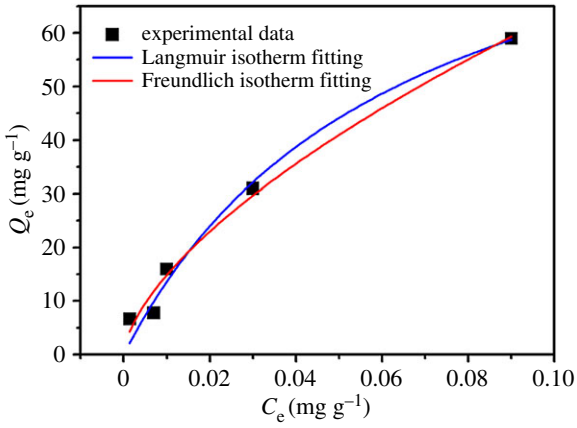

Figure 1. Adsorption isotherm experiment and the fitting result by Langmuir and Freundlich isotherm models for Cry protein adsorption by nano-$Mg(OH)_2$.

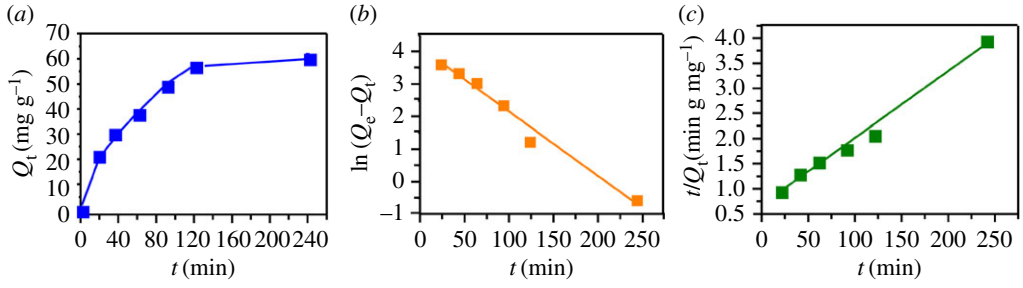

Figure 2. (*a*) Adsorption of Cry11Aa by nano-$Mg(OH)_2$ as a function of contact time (Cry concentration 0.68 g/l, nano-$Mg(OH)_2$ dosage 10 g/l); (*b*) pseudo-first order plot; (*c*) pseudo-second order plot.

Table 1. The Langmuir and Freundlich isotherm model constants for adsorption of Cry11Aa by nano-$Mg(OH)_2$.

	Q^0 (mg g^{-1})		b (l mg^{-1})		
Langmuir	value	s.e.	value	s.e.	R^2
	100.20	16.95	15.74	5.12	0.98
	k		n		
Freundlich	value	s.e.	value	s.e.	R^2
	270.54	44.40	1.59	0.14	0.98

3.2. Effect of time and adsorption kinetics study

The adsorption capacity between Cry11Aa and nano-$Mg(OH)_2$ was evaluated by adsorption kinetics experiments. Figure 2*a* indicated that the rate of Cry11Aa adsorption by nano-$Mg(OH)_2$ is rapid in the first 2 h. The adsorption of protein followed a gradual increase approaching the adsorption equilibrium, and the adsorption capacity could reach as high as 60.6 mg g^{-1}. Meanwhile, pseudo-first (figure 2*b*) and -second order models (figure 2*c*) were used to evaluate the experimental data, and the kinetic parameters calculated by linear regression are given in table 2. The regression coefficients (R^2) for the pseudo-first and -second order models are around 0.98, indicating that both the pseudo-first and -second order equations can fit well with the experimental data. In addition, the examined adsorption capacity (60.6 mg g^{-1}) was closer to the Q_e values which were calculated by the pseudo-first and -second order kinetic models (62.30 and 75.36 mg g^{-1}).

The pseudo-first (3.3) and -second (3.4) order kinetic models are expressed as:

$$\ln(Q_e - Q_t) = \ln Q_e - k_1 t \tag{3.3}$$

$$t/Q_t = 1/k_2 {Q_e}^2 + t/Q_e \tag{3.4}$$

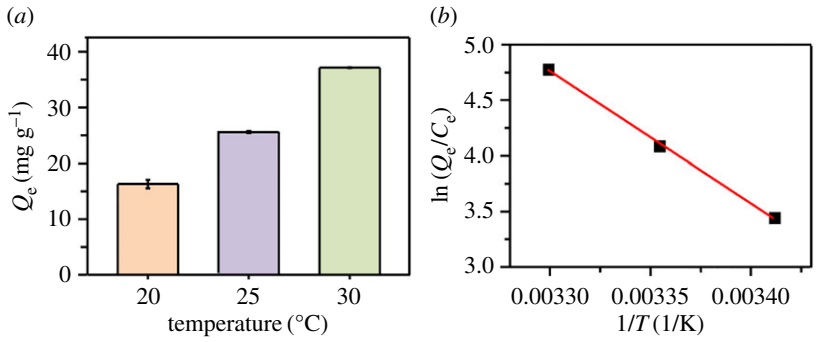

Figure 3. (*a*) Effect of temperature on Cry protein loading, ±s.d. shown by the error bar. (*b*) Plots of ln (Q_e/C_e) versus 1/*T* for the adsorption of Cry11Aa onto nano-Mg(OH)$_2$.

Table 2. The pseudo-first order kinetic and pseudo-second order kinetic constants for adsorption of Cry11Aa by nano-Mg(OH)$_2$.

	Q_e (mg g^{-1})	k g/(mg·min)	R^2
first-order kinetic	62.30	0.0198	0.975
second-order kinetic	75.36	2.56×10^{-4}	0.986

where Q_e and Q_t are the adsorbed amount of protein at equilibrium or at any time (mg g^{-1}), respectively; k_1 (min^{-1}) and k_2 (g mg^{-1} min^{-1}) represent the pseudo-first and -second order rate constants.

3.3. Effect of temperature and adsorption thermodynamic study

Additionally, the influence of different temperatures on the adsorption process was carried out. As shown in figure 3*a*, the adsorption capacity (Q_e) gradually increased from 16.31 mg g^{-1} to 37.08 mg g^{-1} with an increase in temperature from 20°C to 30°C. Meanwhile, enthalpy (ΔH, kJ/mol) and entropy (ΔS, J/mol·K) were obtained from the slope and intercept of the plot from the Van't Hoff equation (as depicted in figure 3*b*), and Gibbs free energy (ΔG, kJ/mol) of the present batch adsorption process was calculated from the Gibbs–Helmholtz equation [26,27]:

$$\ln\left(\frac{Q_e}{C_e}\right) = \frac{\Delta S}{R} - \frac{\Delta H}{RT} \tag{3.5}$$

$$\Delta G = \Delta H - T\Delta S \tag{3.6}$$

where Q_e is the adsorbed capacity at equilibrium (mg g^{-1}), C_e is the equilibrium concentration of Cry protein in the solution (mg l^{-1}), Q_e/C_e is the equilibrium constant (l/g), R is the universal gas constant (8.314 J mol^{-1}· K) and T is the absolute temperature (K).

As shown in table 3, the values of ΔG at different temperatures are negative values, which implies that the adsorption process is spontaneous and favourable at 20°C to 30°C [27]. Meanwhile, the negative value of ΔH indicates the exothermic nature of the adsorption, and the Cry protein adsorption is more efficient at 30°C due to the decrease of ΔG that occurs with the rise of temperature [26]. Moreover, we also conducted the adsorption between Cry protein and Mg(OH)$_2$ at high temperature (50 and 60°C), and the result indicated that the adsorption capacity was gradually decreased (from 23.95 mg g^{-1} to 3.13 mg g^{-1}). This implies that the high temperatures are not suitable to adsorption, because the protein may be partially degraded at high temperatures. Therefore, the adsorption temperature should be controlled below 60°C according to the adsorption thermodynamic study.

3.4. The desorption of Cry11Aa protein from nano-Mg(OH)$_2$

In order to evaluate the stability of adsorption of Cry11Aa by nano-Mg(OH)$_2$, a desorption experiment was conducted. Because the loaded complex is intended for practical application in the field, MES was selected as the desorption medium in order to simulate the pH value in the natural environment (pH = 5.6). Figure 4 indicates that the Cry11Aa had stably adsorbed onto the nano-Mg(OH)$_2$ during the seven cycles, and the desorption rate gradually increased from 3.5% to 31.6%. Afterwards the adsorption

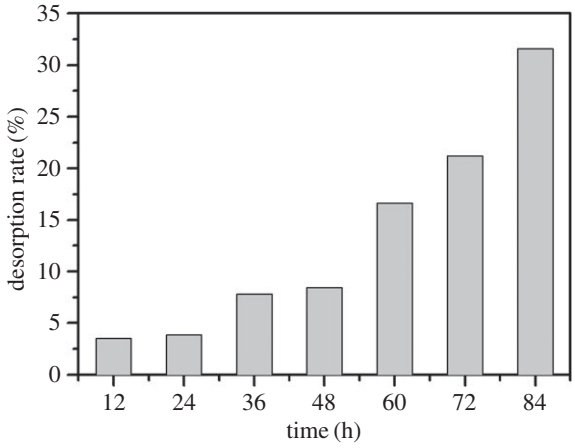

Figure 4. The desorption experiment of Cry11Aa protein from nano-$Mg(OH)_2$ in MES medium. The MES medium was replaced every 12 h, seven times.

Table 3. Thermodynamic parameters for the adsorption of Cry11Aa on nano-$Mg(OH)_2$ at different temperatures.

		ΔG (kJ/mol)		
ΔH (kJ/mol)	ΔS (J/mol· K)	293 K	298 K	303 K
−98.63	365.07	−205.60	−207.42	−209.25

capacity gradually reduced, which might be due to a decrease of nano-$Mg(OH)_2$ quantity in the acidic MES medium.

3.5. The functional group, protein structure and zeta potential analysis

To elucidate the possible interface bonding between nano-$Mg(OH)_2$ and Cry11Aa protein, FT-IR spectra were recorded from 4000 cm^{-1} to 400 cm^{-1} (figure 5*a*). For nano-$Mg(OH)_2$, the absorption peaks at 3696.4 cm^{-1} and 448.8 cm^{-1} are the characteristic peaks of Mg–O [28,29], and the absorption peak at 3448.1 cm^{-1} was characterized as the stretching vibration peaks of hydroxyl groups (–OH) from water molecules [28]. Additionally, a weak peak at 1641.8 cm^{-1} was attributed to the bending vibration of water molecules adsorbed on the surface of nano-$Mg(OH)_2$ [28,30], and the absorption peak at 1460–1400 cm^{-1} was also assigned to the Mg–O stretching vibrations or the Mg–O–Mg deformation vibrations [30]. Compared to unloaded nano-$Mg(OH)_2$, in addition to the characteristic stretching vibration peaks of –OH (3439.3 cm^{-1}) and Mg–O groups (3699 and 438 cm^{-1}) of nano-$Mg(OH)_2$, there was a peak at about 1650 cm^{-1} that may be assigned to the $–NH_2$ groups in the loaded sample, which indicates that the Cry protein was adsorbed on the nano-$Mg(OH)_2$. Meanwhile, the intensity of the Mg–O absorption peak (3699 cm^{-1}) decreased significantly, and the weak peak at 877.2 cm^{-1} might belong to the aromatic C–H. Overall, all these findings confirmed that the protein was adsorbed on the nano-$Mg(OH)_2$.

The secondary structure composition of the Cry11Aa protein before and after loading with nano-$Mg(OH)_2$ was further analyzed using circular dichroism (CD) spectroscopy. As shown in figure 5*b*, the Cry11Aa had negative bands at 225 and 209 nm, which is close to the representative pattern of α-helical-rich proteins [31]. But after loading with nano-$Mg(OH)_2$, the representative pattern of Cry protein was shifted to lower wavelength, which implies the secondary structure of protein was changed compared with the untreated Cry11Aa protein.

Figure 5*c* shows the N_2 adsorption–desorption isotherm results at 77.5 K. The type IV isotherm curve with a clear type H_2 hysteresis loop suggests the presence of mesopores [32], and the specific surface area of nano-$Mg(OH)_2$ was 50.1 $m^2\ g^{-1}$ as calculated using a multipoint BET.

The zeta-potential was employed to confirm the interface bonding between nano-$Mg(OH)_2$ and Cry protein. As shown in figure 5*d*, nano-$Mg(OH)_2$ carried negative charges and after incubation of nano-$Mg(OH)_2$ with the highly negatively charged Cry11Aa protein the mixture solution still maintained a negatively charged zeta potential. This result indicates that the binding between nano-$Mg(OH)_2$ and

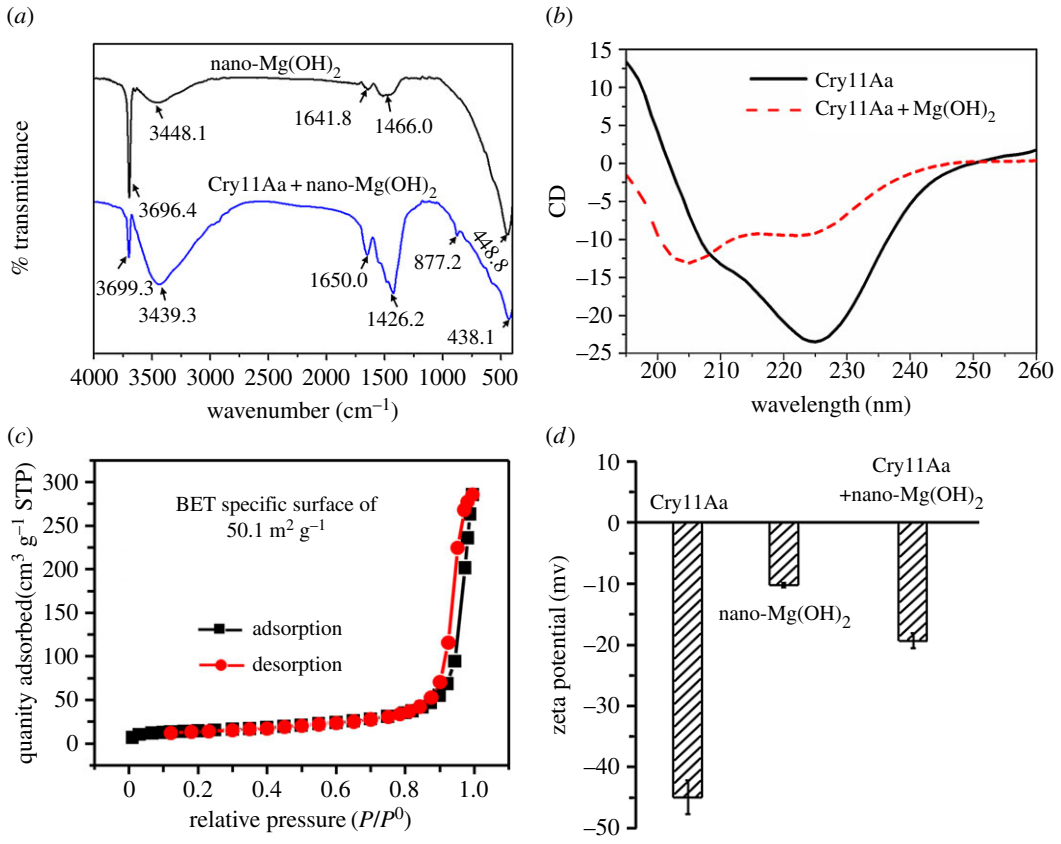

Figure 5. (*a*) FT-IR spectroscopic analysis of nano-$Mg(OH)_2$ and Cry11Aa-$Mg(OH)_2$. (*b*) CD spectra of Cry11Aa proteins before and after loading with nano-$Mg(OH)_2$. The CD spectra of Cry11Aa were obtained after the subtraction of water CD, while the CD spectra of Cry11Aa loading with nano-$Mg(OH)_2$ were obtained after the subtraction of nano-$Mg(OH)_2$ CD. (*c*) N_2 adsorption-desorption isotherms of nano-$Mg(OH)_2$ at 77.5 K and (*d*) zeta-potential of Cry11Aa, nano-$Mg(OH)_2$ and Cry11Aa-$Mg(OH)_2$.

protein could not be driven by electrostatic interactions but might be by covalent linkage, and the decreased potential of nano-$Mg(OH)_2$ loaded with protein also confirmed the protein was adsorbed on the nano-$Mg(OH)_2$.

4. Discussion

The above results have shown that nano-$Mg(OH)_2$ has excellent adsorption ability for Cry11Aa protein. Specifically, the equilibrium concentration was lower than 0.09 mg ml^{-1} as the initial protein concentration was 0.68 mg ml^{-1}, which shows almost complete adsorption of protein is achieved. To obtain a comprehensive understanding of the adsorption behaviour of nano-$Mg(OH)_2$, we further use the Langmuir and Freundlich models to assess the adsorptive ability.

The parameters of the Langmuir model (the saturated adsorption capacity Q^0, adsorption affinity b) are used to characterize the adsorption ability for nano-$Mg(OH)_2$. The saturated adsorption capacity of Cry protein was 100.2 mg g^{-1}, and a higher capacity Q^0 of nano-$Mg(OH)_2$ is beneficial for protein adsorption. Moreover, b is a constant related to the energy of adsorption that reflects the binding strength, and a higher value of b would also be a great help in adsorption. In most studies, several adsorbents have either large Q^0 with small b, or small Q^0 with large b [26]. But our results demonstrate that nano-$Mg(OH)_2$ has large Q^0 and b values, which means that nano-$Mg(OH)_2$ would be an excellent adsorbent in adsorption of Cry protein. Meanwhile, the value of the Freundlich constant n also illustrates that the adsorbate is favourably adsorbed.

The adsorption kinetics study indicated that the adsorption of protein was gradually increased, then approached the adsorption equilibrium after around 2 h. This means that the adsorption could be regulated in a short time in the practical application of nano-$Mg(OH)_2$ as an adsorbent. Previous study also loaded the crystal protein anthelmintic Cry5B with partially oxidized mesoporous silicon (pSi), and

the loading time was 16 h [17]. In our system, the adsorption of Cry11Aa by nano-$Mg(OH)_2$ was a rapid process, and the adsorption capacity could achieve equilibrium in the first 2 h. This excellent adsorption ability might be attributed to the large adsorption affinity of nano-$Mg(OH)_2$ and the relatively high BET areas. Additionally, the adsorption thermodynamic study indicated the exothermic nature of the adsorption; the Cry protein adsorption was more efficient at 30°C, but high temperatures are not suitable for adsorption. This result implied that temperature would be a critical factor in the practical application of nano-$Mg(OH)_2$ as a protein carrier.

The adsorption experiments indicated that the Cry11Aa insecticidal protein could achieve good adsorption on nano-$Mg(OH)_2$, and the adsorption process was driven not by electrostatic interaction but maybe by covalent linkage according to the zeta-potential result. Meanwhile, the FT-IR result showed decreased intensity of Mg-O (approx. 3700 cm^{-1}), which might indicate that the surface Mg-O reacted and was changed; this finding would also support the zeta-potential result that there was covalent linkage between Cry protein and nano-$Mg(OH)_2$.

Our further study on the insecticidal mechanism of the loaded material has indicated that nano-$Mg(OH)_2$ could enhance the proteolysis of Cry protein in mosquito midgut and aggravate the damage to gut epithelial cells [23], and the enhanced toxicity could be attributed to the good adsorption of Cry protein on nano-$Mg(OH)_2$. Therefore, a better understanding of the adsorption behaviour between Cry protein and nano-$Mg(OH)_2$ could provide a basis for assessing nanoadsorbents, which would be a critical step in order to develop a new mosquitocide with high insecticidal activity.

5. Conclusion

In conclusion, this work explored the adsorption features between Cry11Aa and nano-$Mg(OH)_2$. The results indicated that the adsorption process is well fitted to Langmuir and Freundlich isotherm models and followed pseudo-first or -second order rate models; the adsorption was spontaneous and an exothermic process, and high temperatures are not suitable for adsorption. Moreover, the Cry11Aa protein was loaded onto the nano-$Mg(OH)_2$ perhaps through intermolecular forces instead of electrostatic adsorption, and the secondary structure of the protein was changed during the adsorption process. Our work provided details of the adsorption process, which would offer the basic information for use of nano-$Mg(OH)_2$ as a nano-carrier in a practical application.

Data accessibility. All original data are deposited at the Dryad Digital Repository: http://dx.doi.org/10.5061/dryad.08v2c [33].

Authors' contributions. X.P. designed the study, analysed the data and wrote the text. Z.X., Y.Z. and T.H. performed the adsorption isotherm, kinetics and thermodynamic studies. L.L., W.R. and X.H. undertook the FT-IR, CD and zeta potential analysis. S.C., Z.C. and X.G. participated in the manuscript preparation. All authors contributed to its final form and gave final approval for its publication.

Competing interests. We declare we have no competing interests.

Funding. X.G. was supported by the National Key R&D Program of China (No. 2017YFD0200400 and 2011AA10A203), Project of Fujian-Taiwan Joint Center for Ecological Control of Crop Pests (Minjiaoke[2013]51), X.P. was supported by the National Natural Science Foundation of China (31601686), Natural Science Foundation of Fujian Province, China (2016J01112), Fujian Province Education Department, China (JA15156), and Science Fund for Distinguished Young Scholars of Fujian Agriculture and Forestry University, China (Grant xjq201719). Z.C. was supported by the National Natural Science Foundation of China (21607024).

Acknowledgment. We thank Prof. Tianpei Huang and Dr Xiaofeng Xia for their invaluable help in the CD analysis and Mr Qing Cao for assistance with the adsorption data analysis.

References

1. Zhang LL *et al.* 2007 A novel *Bacillus thuringiensis* strain LLB6, isolated from bryophytes, and its new cry2Ac-type gene. *Lett. Appl. Microbiol.* **44**, 301–307. (doi:10.1111/j.1472-765X.2006.02072.x)
2. Zhou XY, Huang QY, Chen SW, Yu ZN. 2005 Adsorption of the insecticidal protein of *Bacillus thuringiensis* on montmorillonite, kaolinite, silica, goethite and Red soil. *Appl. Clay Sci.* **30**, 87–93. (doi:10.1016/j.clay.2005.04.003)
3. Bravo A, Gill SS, Soberon M. 2007 Mode of action of *Bacillus thuringiensis* Cry and Cyt toxins and their potential for insect control. *Toxicon* **49**, 423–435. (doi:10.1016/j.toxicon.2006.11.022)
4. Pan XH, Wu W, Lu J, Chen Z, Li L, Rao WH, Guan X. 2017 Biosorption and extraction of europium by *Bacillus thuringiensis* strain. *Inorg. Chem. Commun.* **75**, 21–24. (doi:10.1016/j.inoche.2016.11.012)
5. Crecchio C, Stotzky G. 2001 Biodegradation and insecticidal activity of the toxin from *Bacillus thuringiensis* subsp. *kurstaki* bound on complexes of montmorillonite–humic acids–Al hydroxypolymers. *Soil Biol. Biochem.* **33**, 573–581. (doi:10.1016/S0038-0717(00)00199-1)
6. Koskela J, Stotzky G. 1997 Microbial utilization of free and claybound insecticidal toxins from *Bacillus thuringiensis* and their retention of insecticidal activity after incubation with microbes. *Appl. Environ. Microbiol.* **63**, 3561–3568.

7. Panbangred W, Pantuwatana S, Bhumiratana A. 1979 Toxicity of *Bacillus thuringiensis* toward *Aedes aegypti* larvae. *J. Invertebr. Pathol.* **33**, 340–347. (doi:10.1016/0022-2011(79)90036-3)
8. Dunkle RL, Shasha BS. 1989 Response of starch-encapsulated *Bacillus thuringiensis* containing ultraviolet screens to sunlight. *Environ. Entomol.* **18**, 1035–1041. (doi:10.1093/ee/18.6.1035)
9. Dunkle RL, Shasha BS. 1988 Starch encapsulated *Bacillus thuringiensis*: a potential new method for increasing environmental stability of entomopathogens. *Environ. Entomol.* **17**, 120–126. (doi:10.1093/ee/17.1.120)
10. Brar SK, Verma M, Tyaci RD, Valero JR. 2006 Recent advances in downstream processing and formulations of *Bacillus thuringiensis* based biopesticides. *Process Biochem.* **41**, 323–342. (doi:10.1016/j.procbio.2005.07.015)
11. Zhang JT, Yan JP, Zheng DS, Sun YJ, Yuan ZM. 2008 Expression of mel gene improves the UV resistance of *Bacillus thuringiensis*. *J. Appl. Microbiol.* **105**, 151–157. (doi:10.1111/j.1365-2672.2008.03729.x)
12. Qin X, Xiang XM, Sun XW, Ni H, Li L. 2016 Preparation of nanoscale *Bacillus thuringiensis* chitinases using silica nanoparticles for nematicide delivery. *Int. J. Biol. Macromol.* **82**, 13–21. (doi:10.1016/j.ijbiomac.2015.10.030)
13. Nair R, Varghese SH, Nair BG, Maekawa T, Yoshida Y, Kumar DS. 2010 Nanoparticulate material delivery to plants. *Plant Sci.* **179**, 154–163. (doi:10.1016/j.plantsci.2010.04.012)
14. Li C, Zhuang Z, Huang F, Wu Z, Hong Y, Lin Z. 2013 Recycling rare earth elements from industrial wastewater with flowerlike nano-$Mg(OH)_2$. *ACS Appl. Mater. Inter.* **5**, 9719–9725. (doi:10.1021/am4027967)
15. Tang F, Li L, Chen D. 2012 Mesoporous silica nanoparticles: synthesis, biocompatibility and drug delivery. *Adv. Mater.* **24**, 1504–1534. (doi:10.1002/adma.201104763)
16. Li ZZ, Chen JF, Liu F, Liu AQ, Wang Q, Sun HY, Wen LX. 2007 Study of UV-shielding properties of novel porous hollow silica nanoparticle carriers for avermectin. *Pest Manag. Sci.* **63**, 241–246. (doi:10.1002/ps.1301)
17. Wu CC, Hu Y, Miller M, Aroian RV, Sailor MJ. 2015 Protection and delivery of anthelmintic protein Cry5B to nematodes using mesoporous silicon particles. *ACS Nano* **9**, 6158–6167. (doi:10.1021/acsnano.5b01426)
18. Wang YJ, Chen JP, Lu LL, Lin Z. 2013 Reversible switch between bulk $MgCO_3 \cdot 3H_2O$ and $Mg(OH)_2$ micro/nanorods induces continuous selective preconcentration of anionic dyes. *ACS Appl. Mater. Inter.* **5**, 7698–7703. (doi:10.1021/am402374e)
19. Liu WZ, Huang F, Wang YJ, Zou T, Zheng JS, Lin Z. 2011 Recycling $Mg(OH)_2$ nanoadsorbent during treating the low concentration of Cr^{VI}. *Environ. Sci. Technol.* **45**, 1955–1961. (doi:10.1021/es1035199)
20. Cao CY, Qu J, Wei F, Liu H, Song WG. 2012 Superb adsorption capacity and mechanism of flowerlike magnesium oxide nanostructures for lead and cadmium ions. *ACS Appl. Mater. Inter.* **4**, 4283–4287. (doi:10.1021/am300972z)
21. Wang ZP, Li CH, Mu Y, Lin Z, Yi AJ, Zhang Q, Yan B. 2015 Nanoadduct relieves: alleviation of developmental toxicity of Cr(VI) due to its spontaneous adsorption to $Mg(OH)_2$ nanoflakes. *J. Hazard. Mater.* **287**, 296–305. (doi:10.1016/j.jhazmat.2015.02.005)
22. Zhang RN *et al.* 2014 Cell rescue by nanosequestration: reduced cytotoxicity of an environmental remediation residue, $Mg(OH)_2$ Nanoflake/Cr(VI) adduct. *Environ. Sci. Technol.* **48**, 1984–1992. (doi:10.1021/es404934f)
23. Pan X *et al.* 2017 Adsorption of insecticidal crystal protein Cry11Aa onto nano-$Mg(OH)_2$: effects on bioactivity and anti-ultraviolet ability. *J. Agric. Food Chem.* **65**, 9428–9434. (doi:10.1021/acs.jafc.7b03410)
24. Pan XH, Wang YH, Chen Z, Pan DM, Cheng YJ, Liu ZJ, Lin Z, Guan X. 2013 Investigation of antibacterial activity and related mechanism of a series of nano-$Mg(OH)_2$. *ACS Appl. Mater. Inter.* **5**, 1137–1142. (doi: 10.1021/Am302910q)
25. Helassa N, Quiquampoix H, Noinville S, Szponarski W, Staunton S. 2009 Adsorption and desorption of monomeric Bt (*Bacillus thuringiensis*) Cry1Aa toxin on montmorillonite and kaolinite. *Soil Biol. Biochem.* **41**, 498–504. (doi:10.1016/j.soilbio.2008.12.008)
26. Cao Q, Huang F, Zhuang Z, Lin Z. 2012 A study of the potential application of nano-$Mg(OH)_2$ in adsorbing low concentrations of uranyl tricarbonate from water. *Nanoscale* **4**, 2423–2430. (doi:10.1039/c2nr11993e)
27. Naskar A, Guha AK, Mukherjee M, Ray L. 2016 Adsorption of nickel onto *Bacillus cereus* M116: a mechanistic approach. *Sep. Sci. Technol.* **51**, 427–438. (doi:10.1080/01496395.2015.1115069)
28. Wang SY, He WZ, Liu C, Li GM, Zhang FE. 2016 Characterizations and preparation of $Mg(OH)_2$ nanocrystals through ultrasonic-hydrothermal route. *Res. Chem. Intermediat.* **42**, 4135–4145. (doi:10.1007/s11164-015-2264-2)
29. Lan SJ, Li LJ, Xu DF, Zhu DH, Liu ZQ, Nie F. 2016 Surface modification of magnesium hydroxide using vinyltriethoxysilane by dry process. *Appl. Surf. Sci.* **382**, 56–62. (doi:10.1016/j.apsusc.2016.04.119)
30. Mahmoud HR, Ibrahim SM, El -Mona SA. 2016 Textile dye removal from aqueous solutions using cheap MgO nanomaterials: adsorption kinetics, isotherm studies and thermodynamics. *Adv. Powder Technol.* **27**, 223–231. (doi:10.1016/j.apt.2015.12.006)
31. Huang T, Zhang X, Pan J, Su X, Jin X, Guan X. 2016 Purification and characterization of a novel cold shock protein-like bacteriocin synthesized by *Bacillus thuringiensis*. *Sci. Rep.* **6**, 35560. (doi:10.1038/srep35560)
32. Hong Y, Zhang J, Huang F, Zhang J, Wang X, Wu Z, Lin Z, Yu J. 2015 Enhanced visible light photocatalytic hydrogen production activity of CuS/ZnS nanoflower spheres. *J. Mater. Chem. A* **3**, 13 913–13 919. (doi:10.1039/C5TA02500A)
33. Pan X *et al.* 2017 Data from: The adsorption features between insecticidal crystal protein and nano-$Mg(OH)_2$. Dryad Digital Repository. (http://dx.doi.org/10.5061/dryad.08v2c)